



## Subsonic Jet Pump Comparative Analysis

*George Bogdan GHERMAN*  
*Scientific Researcher*

*National Research and Development Institute for Gas Turbines COMOTI*  
*220 D Iuliu Maniu Bd., sector 6, cod 061126, OP 76, CP174, Bucharest, Romania*  
[\*bogdan.gherman@comoti.ro\*](mailto:bogdan.gherman@comoti.ro)

*Florin FLOREAN*  
*Scientific Researcher*

*Ionut PORUMBEL*  
*Scientific Researcher*

### ABSTRACT

The paper presents the numerical and experimental studies carried out to optimize, from an aerodynamic point of view, a subsonic jet pump used on aircraft. The optimization of the subsonic jet pump will be done from the aerodynamic, aiming to re-design it such as to reduce as much as possible the emitted noise levels. For this, in a first stage, a parametric set of Reynolds Averaged Navier - Stokes numerical simulation was used on several possible designs, starting from an existing baseline, and including it. The goal was to identify the trends in the flow behavior when key baseline design parameters were varied. During the second stage, aerodynamic measurements were carried out on the two selected configurations and on the baseline configuration for the determination of the instantaneous flow velocity field. The measurements were carried out using cutting edge experimental measure techniques, namely Particle Image Velocimetry. The paper presents a comparison of the numerical and the experimental results and the conclusions of the analysis of the results.

**KEYWORDS:** *jet pump, subsonic, experimental test rig, RANS, efficiency calculation*

### NOMENCLATURE

Latin

$D$  - primary jet nozzle diameter [-];

$PT$  - total pressure [-];

$Q$  - mass flow rate;

$TT$  - total temperature;

$\gamma$  - adiabatic exponent [-];

## 1 INTRODUCTION

Jet pumps applications extent over a wide range of domains from aerospace industry to fire protection industry. Simple and robust design generates performance with low capital cost, ease of maintenance and operation. In the recent years their domain of applicability expanded in areas such as refrigeration and air conditioning systems [1]. They can be use in single phase application or two – phase, like steam driven jet pumps for thermal plants [3].

The principle of operation of a jet pump it is relatively simple, a high velocity fluid it is used to entrain a low pressure fluid and pump it to a higher pressure [2]. There are two types of jet pumps: annular jet pumps (AJP) and central jet pumps (CJP), depending on the nozzle position. As it can be seen in Fig.1 both architectures the design of the jet pump comprises of two cone shape channels, one convergent and one divergent, separated by a straight channel where the mixing between



primary and secondary flow takes place. In the convergent cone channel the secondary flow it is entrained by the high velocity jet from the primary flow and in the second cone, the divergent one, the velocity it is reduced and static pressure increased. Another classification of the jet pumps can be done depending on the fluid working regime, subsonic or supersonic. The later category of jet pumps it is more difficult to create due to shock development and interaction, adverse boundary layer detachment or high turbulent mixing. These things must take into consideration when a supersonic jet pump it is created [3].

The development of these jet pumps, subsonic or supersonic ones, is based more and more on the CFD analysis that can optimize pump efficiency [4].

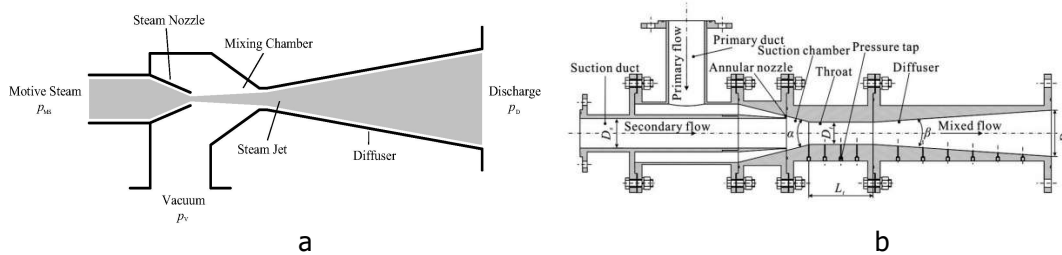


Fig. 1 Jet pump configurations: a) Central jet pump (CJP); b) Annular jet pumps (AJP)[4],[5]

The optimization process involved several stages. First, a number of ten different geometries where proposed and studied, numerically, [5], [6], based on the aerodynamic calculations two of the most promising geometries where after that tested experimentally [6] at the final stage, Fig. 2.

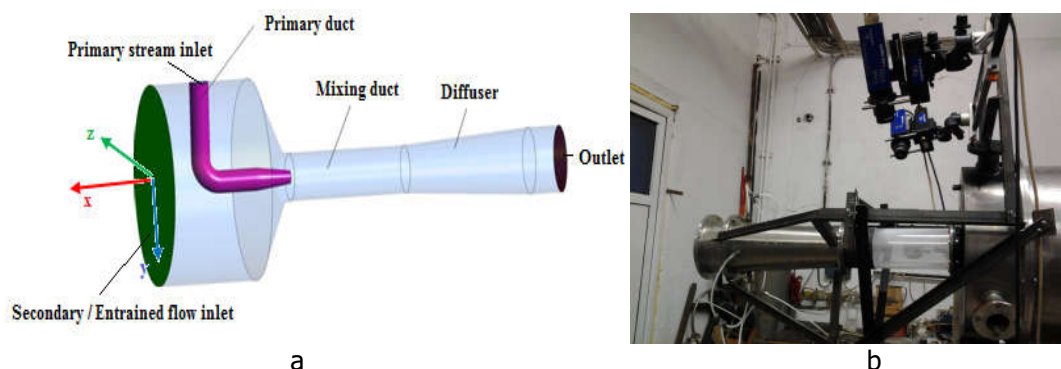


Fig. 2 Jet pump geometry: a) numerical set-up [6]; b) experimental set-up

The optimization process involved several stages and concentrated on the influence of the primary jet pipe length and Chevron effects. First a baseline geometry, which is the property of Liebherr Aerospace, was analyzed and the drawbacks where identified. Secondly, a number of ten different geometries where proposed and studied numerically, [6], [7], based on the aerodynamic calculations two of the most promising geometries where after that tested experimentally [6] at the third and final stage.

This study was disseminated through several papers, [6], [7], [8], and each of these papers presented a part of this elaborate study. The present paper will disseminate the comparison between the experimental and numerical results.

## 2 NUMERICAL SETUP

For the numerical simulation setup it was necessary to discretize the computational domain. From this standpoint, the assessment of the geometry showed a primary jet that exits the ejector pipe and mixes with the entrained mass flow coming from the secondary location. Therefore, it is important to capture boundary layer detachment from the ejector pipe, inner wall and outer wall, and capture mixing between primary and secondary flow inside mixing duct and diffuser. That means a



proper turbulent model must be selected that can properly capture boundary layer detachment and grid resolution must be sufficiently fine close to the walls,  $y^+ \sim 1$ .

For this analysis ANSYS CFX software was used and with the help of ICEM program a structured grid has been done using the blocking structure in order to control the size and length of the cell size close to the walls, see Fig. 3. The turbulence model used was Shear-stress transport (SST)  $k-\omega$  based model [9]. The analysis was steady state (RANS) due to the fact that no temporal non-uniformities of the flow are expected to appear.

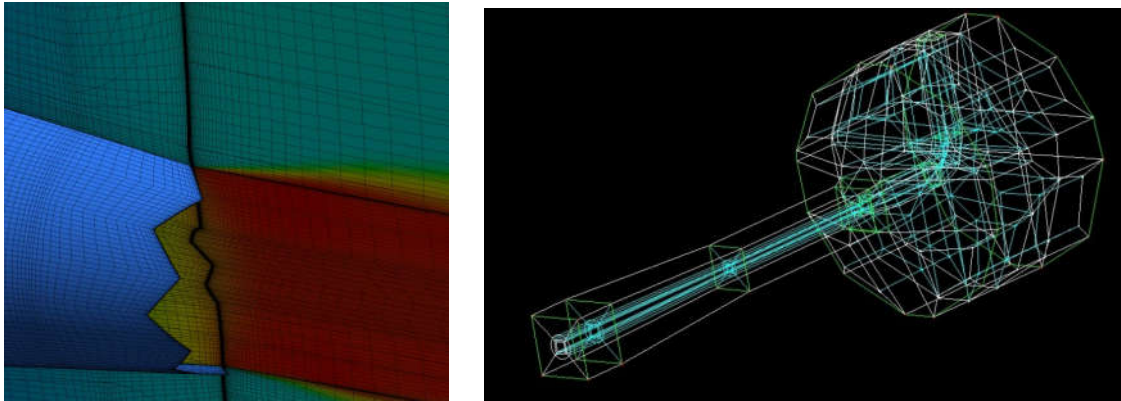


Fig. 3 Computational grid for the Chevron geometry

The coordinate system origin for both of analysis experimental and numerical is at the intersection between centrelines of the primary jet pipe, horizontal and vertical, Fig. 2.

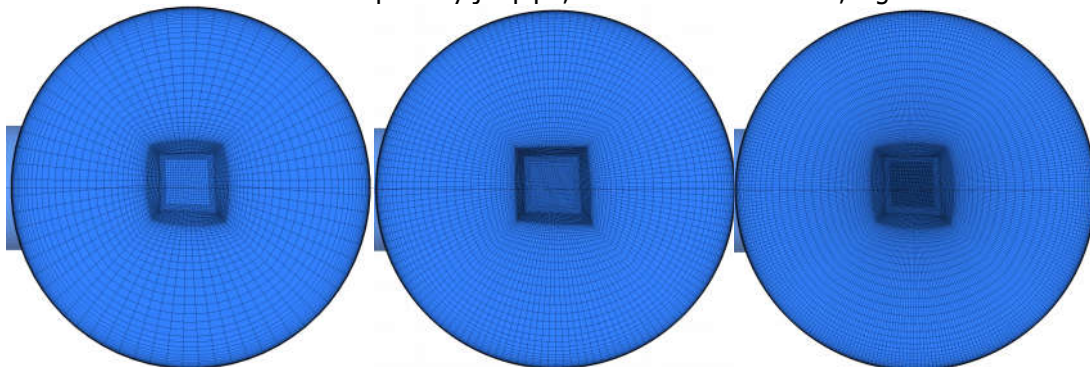


Fig.3.1 Computational for grid for coarse, baseline and fine case

The grid dependency has been performed and the error between the baseline mesh and the finer mesh is lower than 3%. In Fig. 3.1 it can be seen all three grids on which the grid dependency calculations have been performed.

The boundary conditions for these numerical simulations are the same for all the cases, namely, at inlet static pressure and total temperature are specified and at the outlet, atmospheric static pressure, at the walls no-slip condition and adiabatic walls was imposed. The geometry size and values for inlet static pressures and total temperatures can not be disseminated and were determined by Liebherr Aerospace Company [10].

### 3 EXPERIMENTAL SETUP

The combustion chambers test facility was used to perform the experimental measurements. This facility exists at COMOTI, and can provide the mass flow, pressure and temperatures necessary for this geometry while it filters and dry the air. Also, the facility has a stereo LaVision PIV system that was used to capture the instantaneous velocity field inside the jet pump demonstrators, Fig. 4. This PIV system works with the so-called seeding of the working fluid method, meaning the insertion of solid particles in the flow. In this case, Titanium Oxide was used. The PIV system consists of (Fig. 4):



- A double pulsed Nd:YAG Litron LASER of 1200 MJ power and 532 nm wavelength, that provides the basic coherent light used to illuminate the seeding particles at known time intervals;
- Two ICCD cameras that capture the LASER light, placed above the symmetry plane in such a way that two lines of view towards the measurement plane form a 90° angle;
- Mirrors and light sheet optics that capture the LASER beam, reflect it into the proper position, first vertically up, to raise it to the demonstrator centerline, and next horizontally, towards the demonstrator, and transform the beam into a coherent light sheet placed in a horizontal plane along the baseline demonstrator symmetry axis;
- The seeding system, consisting in a Particle Blaster 200 fluidized bed particle injector [11] that provides a Titanium Oxide particles flux.

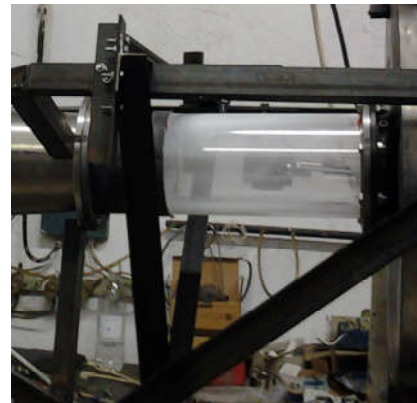


Fig. 4 PIV system and measurement section

Aside from the PIV measurements, pressure, temperature, and mass flow measurements were carried out for purposes of recording the atmospheric conditions, verifying the parameters of the primary and secondary air streams.

A standard barometer and thermometer were placed near the secondary air stream inlet to measure the atmospheric pressure, respectively temperature during the experimentation. Both instruments were placed outside of the secondary air flow path, in order to avoid interference with the air flow. The primary air stream total pressure and temperature were measured by means of pressure probes and thermocouples using the test rig facility standard instrumentation, [12]. The secondary air stream temperature was measured by means of a thermocouple placed immediately upstream of the baseline demonstrator inlet, as shown in Fig. 5. The primary air stream mass flow rate was measured by means of a Venturi tube which is part of the test rig facility standard instrumentation, [13]. A calibrated air inlet equipped with four static pressure measurement ports distributed circumferentially at 90° from each other was placed at the secondary air stream inlet to allow the measurement of the secondary air flow, as shown in Fig. 5. Four static pressure probes were placed at the baseline demonstrator outlet, distributed circumferentially at 90° from each other to allow the calculation of the total air mass flow rate, as shown in Fig. 5. In the mixing region, immediately upstream of the quartz tube, four Kulite instantaneous static pressure probes were placed distributed circumferentially at 90° from each other. The calibrated acquisition frequency of the instantaneous pressure probes was of 3 Hz.

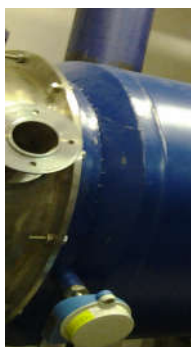


Fig. 5 Temperature probe, static probes placement on the secondary air stream inlet and at jet pump exit

After acquiring the stereo PIV double images using the two ICCD cameras, the images were processed using the DAVIS software, [14], in order to determine the instantaneous velocity field.

#### 4 RESULTS

In order to compare the experimental results with the numerical ones it is necessary to extract data from the both results at the same positions. Due to experimental setup, the measurement plane it is tilted with  $20^\circ$  from Z axis, see Fig. 6, Fig. 7. Accordingly, the data extraction lines are on this plane, at one exit primary pipe diameter, at two exit primary pipe diameter and at three diameters.

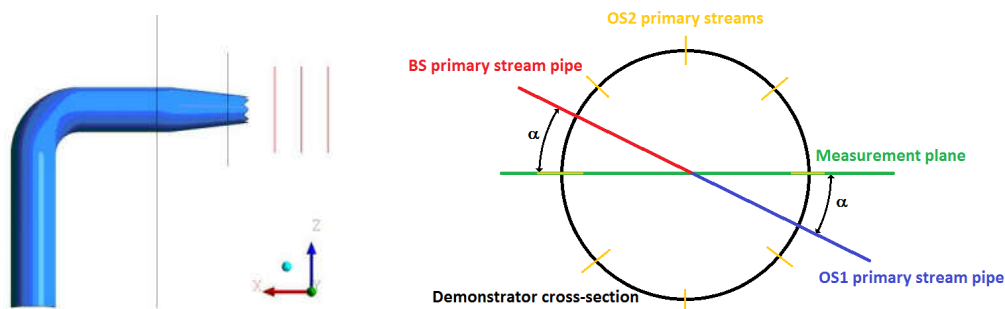


Fig. 6 Lines position (red ones) and plane position in jet pump domain<sup>7</sup>

The center of measurement section it is situated at 0.097 m from the exit of the primary jet, in Fig. 7 it can be seen the position on the numerical plane obtain from CFD analysis.

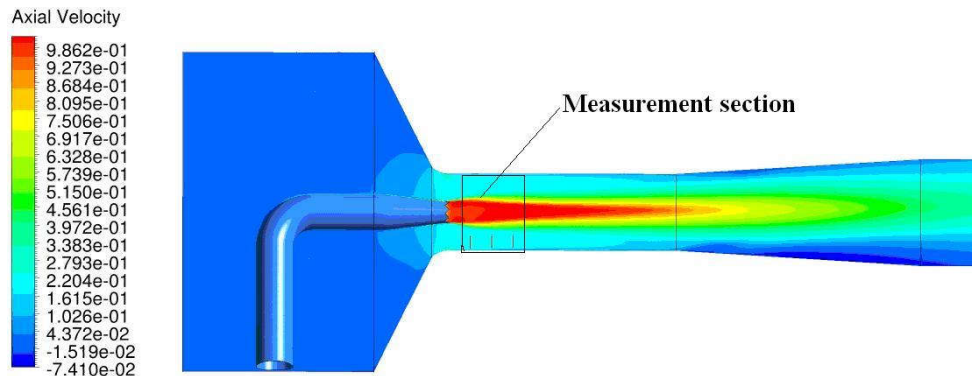


Fig. 7 The PIV measurement section position in the domain

Although the measurement section covers mixing section from wall to wall, as it can be seen in Fig. 7, the results are corrupted towards the walls of this section, as it can be seen in Fig. 8, it is possible to observe pockets of white color that indicate regions where light it is reflected and generate errors in measurement. That is why these regions must be eliminated from the results file. Also, it was not possible to capture correctly the boundary of the primary jet, experimentally, as it can be seen in Fig. 8 (right figure), thus identifying the mixing region properly. Also, the standard deviation of the measured experimental data is approximately 20 %.

Thus, the measurement lines extend only for a distance of 0.05 m from the entire mixing section diameter which is 0.125 m. Also, the velocity and vorticity are adimensionalised with a reference velocity, 320 m/s. The distance on which these measurements are taken is adimensionalised by the mixing section diameter, 0.125 m.

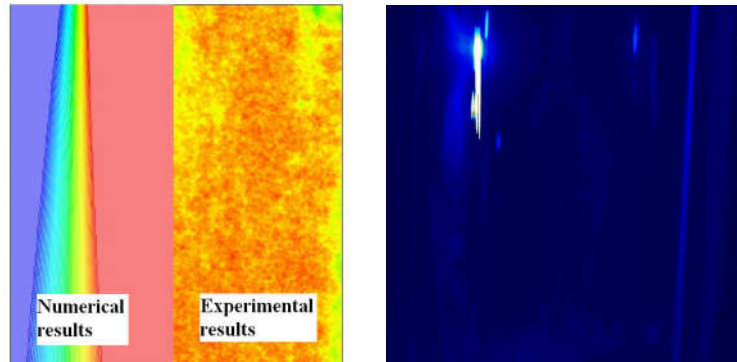


Fig. 8 Comparison of axial velocity distribution inside jet pump (right), experimental field captured by one of the ICCD cameras (left)

Nevertheless, the comparisons between the experimental and numerical results reveal interesting aspects that will be described in the following section.

The results are compared for three cases, namely baseline, the original geometry, the two diameters shorter primary pipe case and the Chevron case, where the baseline primary jet pipe it is equipped with 8 Chevrons with an  $90^\circ$  degrees angle. It is also necessary to mention that the following section of the primary jet pipe it is situated on the left of the graphs, see Fig. 6 (left).

As it can be seen, in Fig. 9, 10 and 11, the velocity of primary jet potential core it was estimated correctly by the RANS simulations, however some fluctuations appear, in the Chevron case the shape of the fluctuation might suggest a influence from the chevron geometry. Also, it is observed that the boundary of the jet potential core it can not be verified in these experimental results. The velocity distribution inside jet potential core it is smoother in the 2D short case.

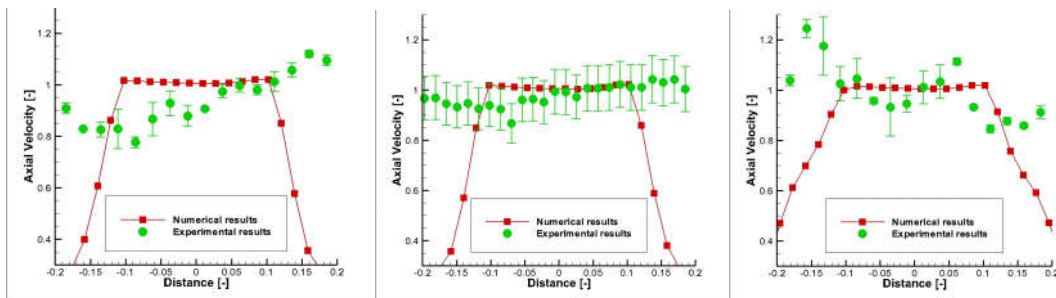


Fig. 9 Axial velocity distribution at 1D from the primary section outlet for the baseline (a), 2D short (b) and chevron case (c)

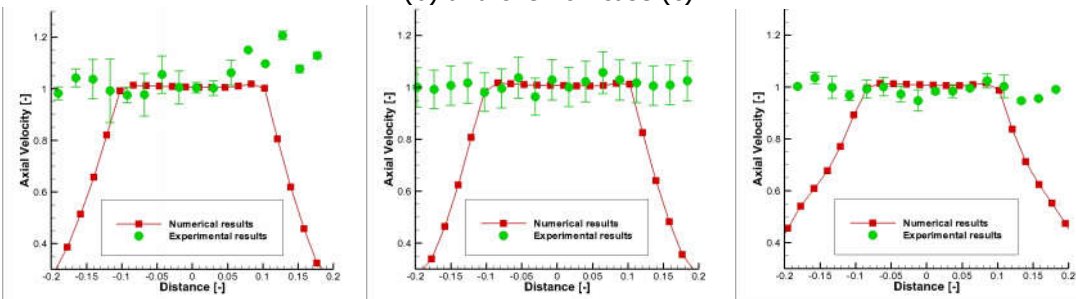


Fig. 10 Axial velocity distribution at 2D from the primary section outlet for the baseline (a), 2D short (b) and chevron case (c)

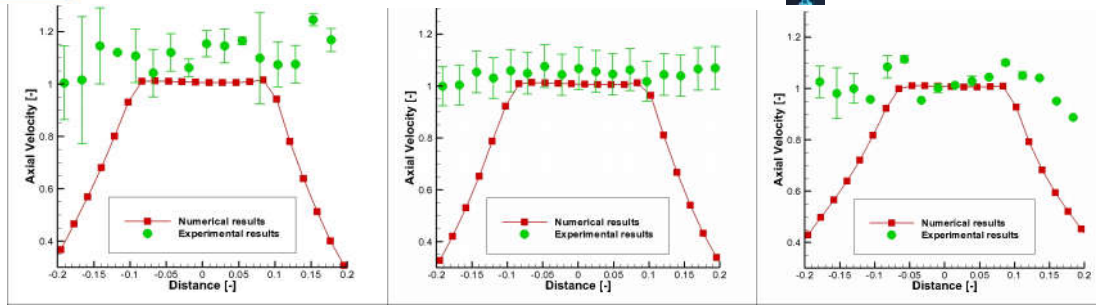


Fig. 11 Axial velocity distribution at 3D from the primary section outlet for the baseline (a), 2D short (b) and chevron case (c)

The radial velocity profile shows accentuated discrepancies between numerical results and experimental ones in the baseline and Chevron case. These differences tend to smooth out as the distance from the primary jet exit increases, see Fig. 12, 13 and 14. Another interesting aspect is observed on the left of the graphs, where the presence of the vertical section of the pipe has a major influence on the flow field, see Fig. 15, influence, which it is not well captured by the RANS simulations. Also, radial velocity profile resembles in both results, but the amplitude of the velocity fluctuations is stronger in the experimental results and smooth out as the distance from the primary exit pipe increases.

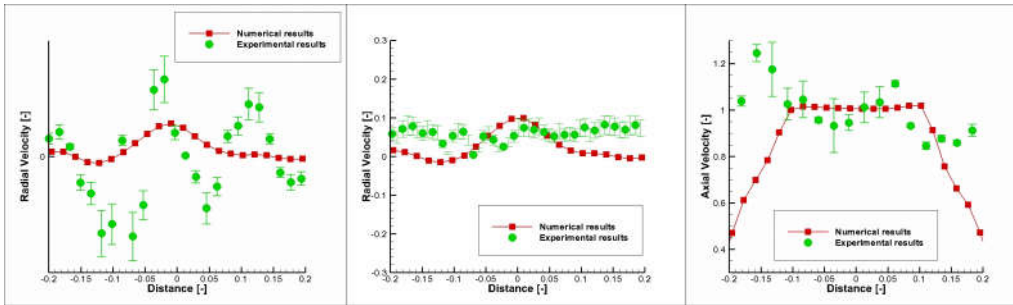


Fig. 12 Radial velocity distribution at 1D from the primary section outlet for the baseline (a), 2D short (b) and chevron case (c)

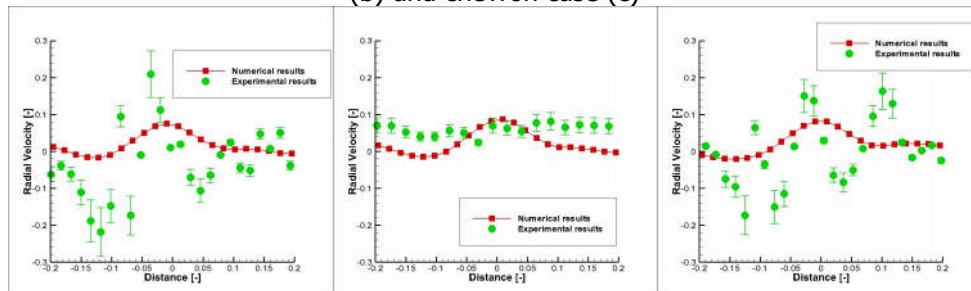


Fig. 13 Radial velocity distribution at 2D from the primary section outlet for the baseline (a), 2D short (b) and chevron case (c)

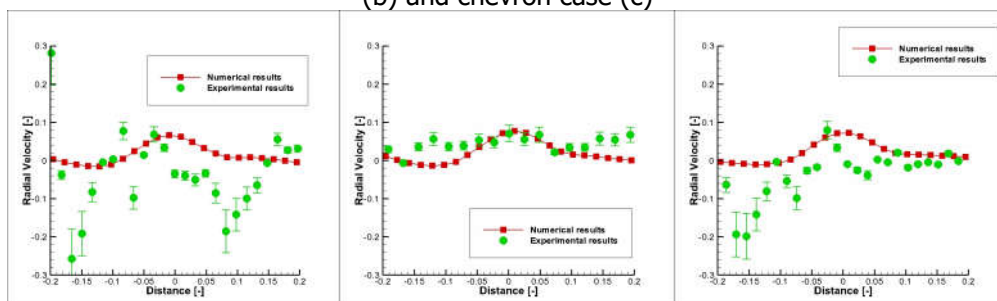


Fig. 14 Radial velocity distribution at 3D from the primary section outlet for the baseline (left), 2D short (center) and chevron case (right)

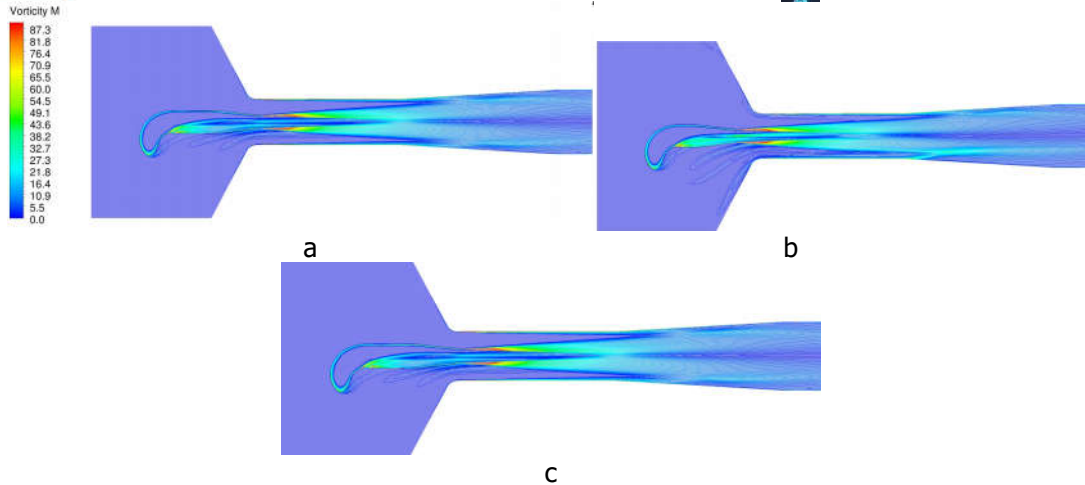


Fig. 15 Vorticity plot in the jet pump numerical domain: a) baseline, b) 2D short case, c) chevron case

The vorticity plots reveal that the amplitude of the fluctuations at the same level for both experimental and numerical results, see Fig. 16, 17 and 18. However it is not possible to distinguish a profile of the vorticity distribution in case of the experimental results.

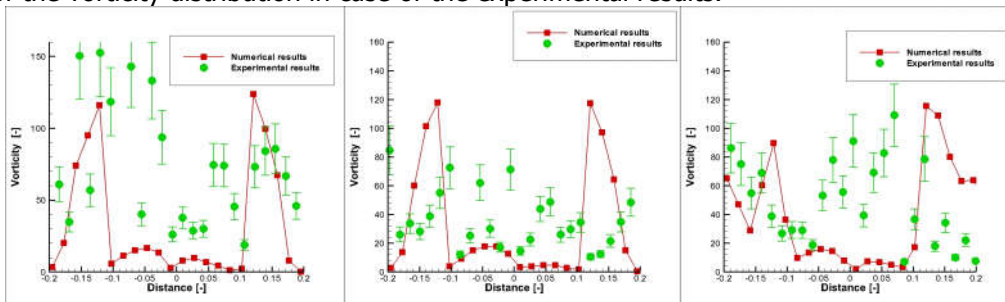


Fig. 16 Vorticity distribution at 1D from the primary section outlet for the baseline (a), 2D short (b) and chevron case (c)

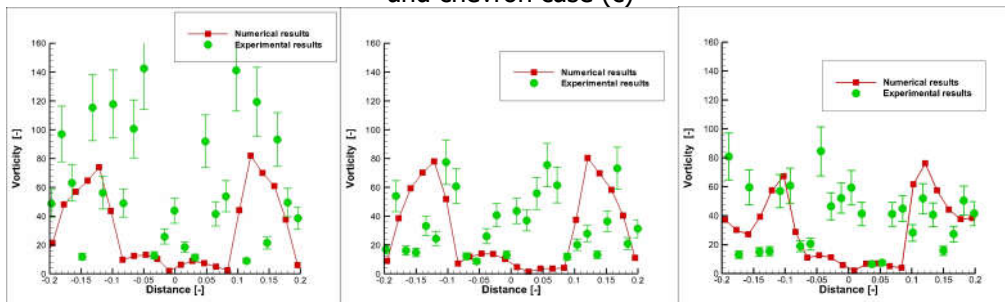


Fig. 17 Vorticity distribution at 2D from the primary section outlet for the baseline (a), 2D short (b) and chevron case (c)

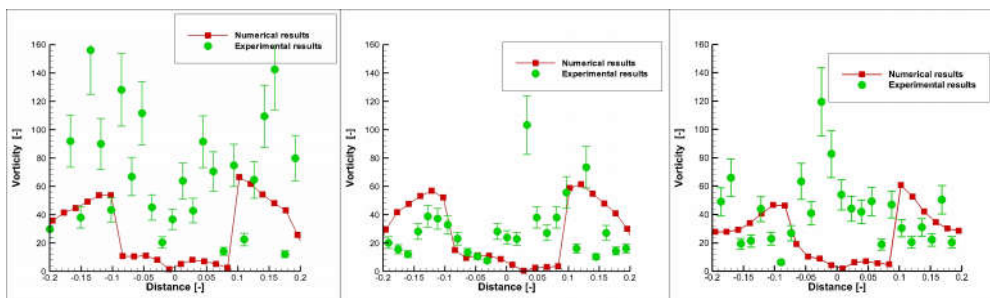


Fig. 18 Vorticity distribution at 3D from the primary section outlet for the baseline (a), 2D short (b) and chevron case (c)



To calculate an efficiency of the proposed solutions, Liebherr specialists developed the following formula:

$$\eta = \frac{Q_2}{Q} \cdot \frac{TT_2}{TT_1} \cdot \frac{\left(\frac{PT_5}{PT_2}\right)^{\frac{1}{\gamma}} - 1}{\left(\frac{PT_1}{PT_5}\right)^{\frac{1}{\gamma}} - 1}$$

The efficiency obtained for the three case studied shows some differences between the efficiency envisaged by simulations and experiments. Namely, for the baseline, efficiency obtain is 0.314 for the numeric results and 0.222 for the experimental results, for the 2D short case the efficiency is 0.297 for the numerical results and 0.305 for the experimental results and finally for the Chevron case, efficiency obtain is 0.317 for the numerical results and 0.225 for the experimental results.

## 5. CONCLUSIONS

Numerical and experimental aerodynamic analysis has been carried out on three jet pump geometries to asses the impact of optimization solutions on the baseline geometry. The two optimization solutions studied, concern the reduction of the primary jet pipe length with two diameters and second the usage of chevrons on the exit of the primary jet pipe. The chevron consists of 8 teeth with an opening of 90° degrees. The numerical simulations were performed using a RANS and the experimental analysis was performed using PIV. The comparison between the two analyses shows good agreement and validates the numerical simulation. Also the efficiency computed for the experimental part it is based on the pressure, temperature and mass flow probes that were used auxiliary to PIV system, which are described in the paper. Although the potential core of the primary jet it is not well captured by the experiments, the axial velocity, radial velocity and vorticity profile shows good agreements in most of the graphs. In conclusion the best optimized efficiency it is observed at the two diameter short case.

## ACKNOWLEDGMENTS

The work presented in the paper was carried out under the FP 7 Clean Sky research project no. 325977 - OPA. The authors would like to thank Liebherr specialists for their support.

## REFERENCES

1. Perry and Green - R.H. Perry, D.W. Green (Eds.), Perry's Chemical Engineers' Handbook Chemical engineers' handbook, McGraw-Hill, New York, NY (1997)
2. J. Fan, J. Eves, H.M. Thompson, V.V. Toropov, N. Kapur, D. Copley, A. Mincher + Computational fluid dynamic analysis and design optimization of jet pumps, Computers & Fluids journal, Volume 46, Issue 1, Pages 212-217, July 2011.
3. Stefan Brendelberger, Henrik von Storch, Brendan Bulfin, Christian Sattler - Vacuum pumping options for application in solar thermochemical redox cycles – Assessment of mechanical-, jet- and thermochemical pumping systems, Solar Energy journal, Volume 141, Pages 91-102, 1 January 2017
4. S. He, Y. Li, R.Z. Wang - Progress of mathematical modeling of ejectors, Renew Sustain Energy Rev, 13 (2009), pp. 1760-1780, 2009
5. Mao-sen Xu, Xue-long Yang, Xin-ping Long, Qiao Lü - Large eddy simulation of turbulent flow structure and characteristics in an annular jet pump, Journal of Hydrodynamics, 29(4):702-715 DOI: 10.1016/S1001-6058(16)60782-5, 2017
6. B. Semlitsch, E. Laurendeau, and M. Mihaescu, "Steady-State and Unsteady Simulations of a High Velocity Jet into a Venturi Shaped Pipe", Proceedings of the 4th Joint US-European Fluids Engineering Summer Meeting, FEDSM 2014, August 3-7, 2014, Chicago, IL, USA, FEDSM2014-22162.
7. F. G. Florean, A. C. Petcu, I. Porumbel, G. Dediu - PIV measurements in Low Noise Optimized Air Jet Pump Demonstrators,



8. B. G. Gherman, I. Malael, M. Mihaescu, and I. Porumbel, "Jet Pump Optimization through Reynolds Averaged Navier-Stokes Simulation Analysis", *AIAA 22<sup>nd</sup> Computational Fluid Dynamics Conference*, Dallas, TX, USA, 2015.
9. B. Semlitsch, E. Laurendeau, and M. Mihaescu, "Steady-State and Unsteady Simulations of a High Velocity Jet into a Venturi Shaped Pipe", *Proceedings of the 4th Joint US-European Fluids Engineering Summer Meeting, FEDSM 2014*, August 3-7, 2014, Chicago, IL, USA, FEDSM2014-22162.
10. Menter F.R., "Two-equation eddy-viscosity turbulence models for engineering", *AIAA- Journal*, 32 (8), 1994.
11. Liebherr Aerospace, "Technical Report", T-JTI-ACOUST-SP-0002, 22.04.2013, unpublished.
12. LaVision GmbH "Particle Blaster 200, Product Manual", 2008.
13. I. Porumbel, K. Knobloch, C.E. Hrițcu, F.G. Florean, C. Sandu, G. Ursescu. "Experimental Measurements for Testing a New Sensor for Acoustic Pressure Measurements in the Hot Regions of a Gas Turbine Engine", *The XXIX "Știința Modernă și Energia" Conference*, Cluj - Napoca, Romania, 2010.
14. LaVision GmbH "DaVis 7.2 Software, Product Manual", 2008.